The use of FWI in coal exploration

Mehdi Asgharzadeh*
Curtin University
Perth, Australia
mehdi.asgharzadeh@curtin.edu.au

Maryam Bahri
Curtin University
Perth, Australia
maryambahri2013@gmail.com

Milovan Urosevic
Curtin University
Perth, Australia
m.urosevic@curtin.edu.au

SUMMARY

Seismic surveys are routinely used for building precise structural images of the coal bearing formations in Australia but coal production related hazards such as weak strata and zones with an increased gas content remain to be fully resolved by seismic measurements. One way of investigating these issues is through the application of Full Waveform Inversion (FWI) methods. To utilise the full power of these methods a high quality seismic dataset is needed. Such conditions are often met by 2D and 3D reflection seismic data acquired over coal seams in Bowen and Sydney basins. FWI can be used for a high resolution estimate of P- and S-wave velocities and the density that can also be translated into geotechnical parameters of interest to mining operations. In this study, we evaluate the applicability of FWI methods for estimating elastic parameters (P and S wave velocities and density) from the inversion of a synthetic seismic dataset that was recorded over the surface of a 2D earth model that represents subsurface geology in Goonyella coal mine in Queensland, Australia. We generated elastic synthetic shot records using finite difference algorithm and inverted these data back for model parameters to assess the potential of the FWI algorithm. Using only a short array of surface receivers (cheaper option), we show that the application of FWI method can still improve the original earth models towards the true solutions. We were also able to reconstruct the elastic boundaries for a major part of the subsurface models within the seismic bandwidth. Interpretation of the estimated parameters for coal mining objectives is then straightforward.

Key words: full waveform inversion, coal exploration, seismic methods, Goonyella mine, Australia.

INTRODUCTION

3D reflection seismic is routinely used for a precise mapping and characterisation of coal seams in Australia (Urosevic et al., 1992, Hatherly et al., 2008). Seismic images are also used to analyse and predict underground hazards such are faults, folds, weak strata, gassy zones, and etc. Structural analysis of 3D seismic images is then utilized to help plan underground mining operations. While time seismic images are of a high quality; issues with depth conversion, fault throw estimate, coal quality, presence of fractured and gassy zones, weak strata, etc. are still to be fully resolved from seismic images. A step change in solving these issues could be by incorporating Full Waveform Inversion (FWI) into seismic borehole and surface imaging flows. The seismic data quality in Bowen and Sydney basins is such that FWI could be applied over a wide frequency band to produce high resolution P-wave and more importantly density images, particularly from VSP data that can be used for both depth imaging and directly for coal characterization.
In this study we evaluate the potential of FWI for coal exploration in Australia by conducting comprehensive, log-derived simulation analysis. We will apply full waveform inversion technique to synthetic shot gathers that were recorded over the surface of a 2D earth model that represents subsurface geology in North Goonyella coal mines in Queensland. In the first part, the theory, we describe fundamental equations behind the FWI technique and show how deviations in data from what is predicted by a guess solution can be related to a model update that is required to move towards the final solution. In the second part, model building, we explain how we built 2D earth models required for the inversion from velocity and density logs in Goonyella mine. In the third part, synthetic data generation, we describe parameterization of the forward model and generation of synthetic shot records that will play the role of field observations in our inversion study. In the last part, full waveform inversion, we describe the parameterization of the inversion flow and discuss the results.

.

THE THEORY

Full Waveform Inversion (FWI) methods aim to estimate the elastic parameters of the underground materials by minimizing the misfit energy between the modelled ($\mathbf{u}^{\mathrm{mod}}$) and filed data ($\mathbf{u}^{\mathbf{obs}}$) using a gradient optimization approach. Utilizing computation power of super computers, FWI methods use the full information content of each recorded seismogram (e.g. reflected waves, refracted waves, surface waves, diving waves, super critical reflections, multiscattered waves such as multiples and etc.) to iteratively improve the resolution of estimated parameters and are capable of resolving sub-seismic structural elements (Pratt et al., 2002). In reflection seismic, the elastic displacement field $\mathbf{u}^{\mathbf{obs}} = u(\mathbf{X_s}, \mathbf{X_r}, t)$ exited by sources located at $\mathbf{X_s}$ will be recorded by receivers at $\mathbf{X_r}$ within the time interval t. For a given model $\mathbf{m}$ of the subsurface, the forward problem (wave equation) can be solved using numerical methods such as finite-differences (Virieux, 1986) and finite-elements (Marfurt, 1984, Min et al., 2003) to estimate model dataset $\mathbf{u}^{\mathrm{mod}}$. A misfit vector can be defined at the receiver positions between the recorded seismic data and the modelled seismograms as $\boldsymbol{\delta}\mathbf{u} = \mathbf{u}^{\mathbf{mod}} - \mathbf{u}^{\mathbf{obs}}$ for each source in the survey. The model represents some physical parameters of the subsurface (e.g. V_P ,V_S , ρ

in the elastic case) discretised over the computational domain. For each seismic source, we can define a least-square norm $E(\mathbf{m})$ of the misfit vector to represent the objective function in the inversion:

$$E(\mathbf{m}) = \frac{1}{2}\boldsymbol{\delta}\mathbf{u}^{\mathbf{T}}\boldsymbol{\delta}\mathbf{u}\,, \qquad \text{(Eq. 1)}$$

where superscript **T** denotes matrix transpose operation. The minimum of the objective function $E(\mathbf{m})$ is typically searched in the vicinity of a starting model $\mathbf{m}^{(p)}$. Information about the shape of the objective function $E(\mathbf{m})$ in the vicinity of $\mathbf{m}^{(p)}$ can help to devise a better solution $\mathbf{m}^{(p+1)}$. Taylors's theorem indicates that the entire function shape at $\mathbf{m}^{(p)}$ can be built from the derivatives of $E(\mathbf{m})$. A second-order Taylor-Lagrange development of the objective function $E(\mathbf{m})$ in the vicinity of the model $\mathbf{m}^{(p)}$ gives (Menke, 1984):

$$E(\mathbf{m}) \approx E(\mathbf{m}^{(p)}) + \sum_{i=1}^{M} b_i (m_i - m_i^{(p)}) + \frac{1}{2}\sum_{i=1}^{M}\sum_{j=1}^{M} B_{ij}(m_i - m_i^{(p)})(m_j - m_j^{(p)}) \qquad \text{(Eq. 2)}$$

With $b_i = \left.\frac{\partial E}{\partial m_i}\right|_{\mathbf{m}^{(p)}}$ and $B_{ij} = \left.\frac{\partial^2 E}{\partial m_i \partial m_j}\right|_{\mathbf{m}^{(p)}}$.

Where the integer M denotes the number of elements in vector $\mathbf{m}$, $\mathbf{b}$ is the vector of first derivatives and $\mathbf{B}$ is a matrix of second derivatives evaluated at trial solution $\mathbf{m}^{(p)}$. These derivatives can be approximated with finite differences as (Menke, 1984):

$$\left.\frac{\partial E}{\partial m_i}\right|_{\mathbf{m}^{(p)}} \approx \frac{1}{\Delta m}\left\{E(\mathbf{m} + \boldsymbol{\Delta}\mathbf{m}^{(\mathbf{i})}) - E(\mathbf{m})\right\}, \qquad \text{(Eq. 3)}$$

$$\left.\frac{\partial^2 E}{\partial m_i \partial m_j}\right|_{\mathbf{m}^{(p)}} \approx \left\{ \begin{array}{l} \dfrac{1}{(\Delta m)^2}\left\{E(\mathbf{m} + \boldsymbol{\Delta}\mathbf{m}^{(\mathbf{i})}) - 2E(\mathbf{m}) + E(\mathbf{m} - \boldsymbol{\Delta}\mathbf{m}^{(\mathbf{i})})\right\}, (i = j) \\ \dfrac{1}{4(\Delta m)^2}\left\{ \begin{array}{l} E(\mathbf{m} + \boldsymbol{\Delta}\mathbf{m}^{(\mathbf{i})} + \boldsymbol{\Delta}\mathbf{m}^{(\mathbf{j})}) - E(\mathbf{m} + \boldsymbol{\Delta}\mathbf{m}^{(\mathbf{i})} - \boldsymbol{\Delta}\mathbf{m}^{(\mathbf{j})}) - E(\mathbf{m} - \boldsymbol{\Delta}\mathbf{m}^{(\mathbf{i})} + \boldsymbol{\Delta}\mathbf{m}^{(\mathbf{j})}) \\ + E(\mathbf{m} - \boldsymbol{\Delta}\mathbf{m}^{(\mathbf{i})} - \boldsymbol{\Delta}\mathbf{m}^{(\mathbf{j})}) \end{array} \right\}, (i \neq j) \end{array} \right\}. \qquad \text{(Eq. 4)}$$

Here, $\boldsymbol{\Delta}\mathbf{m}^{(\mathbf{i})}$ is a small increment in the i^{th} direction.

The minimum of the objective function $E(\mathbf{m})$ can be found by differentiating the approximate equation with respect to a model parameter m_q and setting it to zero:

$$\frac{\partial E(\mathbf{m})}{\partial m_q} = 0 \Rightarrow b_q + \sum_{j=1}^{M} B_{qj}(m_j - m_j^{(p)}) = 0\,, \qquad \text{(Eq. 5)}$$

or

$$\mathbf{m} - \mathbf{m}^{(p)} = -\mathbf{B}^{-1}\mathbf{b}\,. \qquad \text{(Eq. 6)}$$

In the non-linear case ($\mathbf{d} = g(\mathbf{m})$), the error is $E(\mathbf{m}) = [\mathbf{d} - g(\mathbf{m})]^T[\mathbf{d} - g(\mathbf{m})]$ from which we get (Menke, 1984):

$$\mathbf{b} = -2\mathbf{G}^{(p)T}[\mathbf{d} - g(\mathbf{m}^{(P)})]\,, \qquad \text{(Eq. 7)}$$

and

$$\mathbf{B} \approx 2[\mathbf{G}^{(p)T}\mathbf{G}^{(p)}]\,, \qquad \text{(Eq. 8)}$$

with $G_{ij}^{(p)} = \left.\frac{\partial g_i}{\partial m_j}\right|_{m^{(p)}}$, and we finally get:

$$\mathbf{m} - \mathbf{m}^{(p)} \approx [\mathbf{G}^{(p)T}\mathbf{G}^{(p)}]^{-1}\mathbf{G}^{(p)T}[\mathbf{d} - g(\mathbf{m}^{(P)})]\,. \qquad \text{(Eq. 9)}$$

Matrix $\mathbf{G}^{(p)}$ is the gradient of the model $g(\mathbf{m})$ at trial solution (data kernel) and can be approximated by finite differences using equations 3 and 4. The generalized inverse term $\mathbf{G}^{-g} = [\mathbf{G}^{(p)T}\mathbf{G}^{(p)}]^{-1}\mathbf{G}^{(p)T}$ in equation 9 relates the deviation of the data

$\Delta\mathbf{d} = [\mathbf{d} - g(\mathbf{m}^{(P)})]$ from what is predicted by the trial solution to the deviation of the solution $\Delta\mathbf{m} = \mathbf{m} - \mathbf{m}^{(p)}$ from the trial solution that is $\Delta\mathbf{m} = \mathbf{G}^{-g}\Delta\mathbf{d}$. Because this solution was derived for a Taylor approximation of the objective function, it is only approximate, and improvements can be achieved through several iterations (Menke 1984):

$$\mathbf{m}^{(p+1)} = \mathbf{m}^{(p)} + [\mathbf{G}^{(p)T}\mathbf{G}^{(p)}]^{-1}\mathbf{G}^{(p)T}[\mathbf{d} - g(\mathbf{m}^{(P)})]. \qquad \text{(Eq. 10)}$$

Parameter $\mathbf{G}^{(p)T}\mathbf{G}^{(p)}$ is commonly referred to as approximate Hessian and Gauss-Newton methods (Akcelik, 2002, Askan et al., 2007, Askan and Bielak, 2008 and Epanomeritakis et al., 2008) can be used to solve equation 10. However, the more efficient way of solving equation 10 would be by replacing inverse Hessian by a scalar α (the step length) and utilizing gradient methods (Mora, 1987, Tarantola, 1987 and Crase et al., 1990) for minimization.

CONSTRUCTION OF 2D EARTH MODEL FROM WELL LOG MEASUREMENTS

In this study we built two groups of velocity and density earth models from log measurements at the location of well GN-717. Each set of models, contains a separate numerical grid for P-wave velocity, S-wave velocity and the density. First group were aimed to be used in generating seismic shot records that would play the role of field measurements $\mathbf{u}^{\mathbf{obs}}$ in our analysis. We built these (true) models from finely resampled velocity and density logs (1 m block size) by discretising them in the forward modelling grid. The second set of models were aimed to play the role of starting point in the inversion $\mathbf{m}^{(p)}$. We built these models by coarsely resampling the same velocity and density logs (20 m block size) and discretising them in the inversion grids. Figure 1 is an illustration of original (black) and resampled velocity and density logs (blue and red) that were used in building FWI models. We constructed S-wave velocity from P-wave velocity log by applying Castagna et al. (1985) empirical equation for S-wave velocity ($V_S = 0.8619V_P - 1172$).

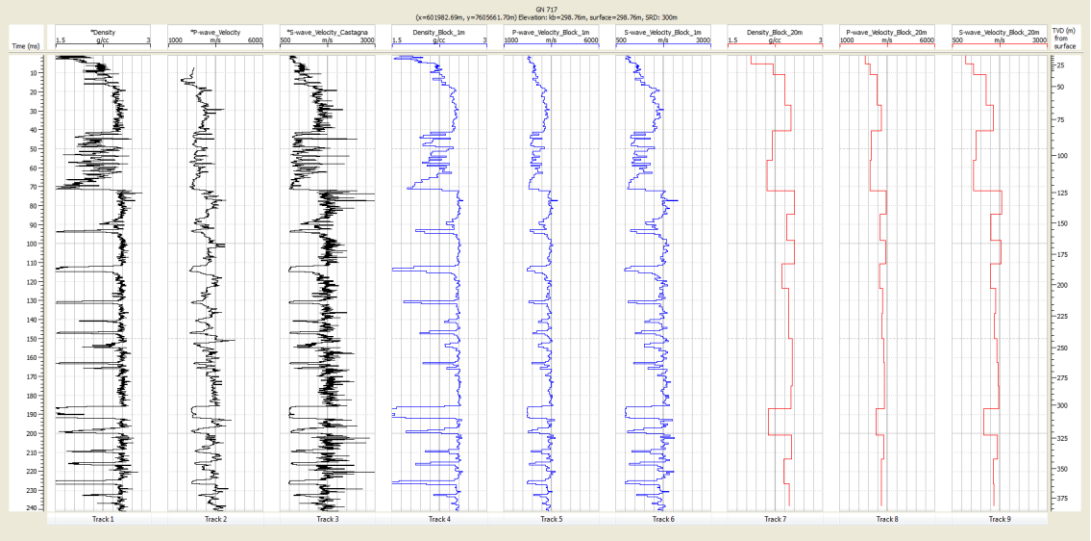

Figure 1: Original and resampled velocity and density logs at well GN717. Logs blocked with 1 m window size (tracks=4-6) were used to build forward modelling grid and production of synthetic shot records. Logs blocked with 20 m window size (tracks=7-9) were used to build the starting model for FWI inversion. Coal bearing intervals can be easily identified by their substantially lower values observed in density logs. Shear velocity log was constructed from P-wave velocity log by applying Castagna et al. (1985) relationship.

We constructed both the true and initial models by discretising the corresponding resampled logs into a 1000×1000 grid with $dh = 0.4$ m spacing in both the vertical and lateral directions. To minimize numerical dispersion, grid size dh was computed as:

$$dh \le \frac{V_{S,\min}}{2 f_c n}. \qquad \text{(Eq. 11)}$$

Grid size is a function of the order of spatial finite difference (FD) operators used in the simulation and the shortest wavelength being simulated ($\frac{V_{S,\min}}{f_{\max}}$, $f_{\max} = 2 f_c$). For 4th order FD operator (used in this analysis), n=8. This resulted in velocity and density models with 400 meters length in either directions. Velocity and density readings at the bottom of the logs (386 m) were continued to the bottom of the models (400 m) as a constant value. Figure 2 demonstrates both the true and initial models used in this inversion analysis.

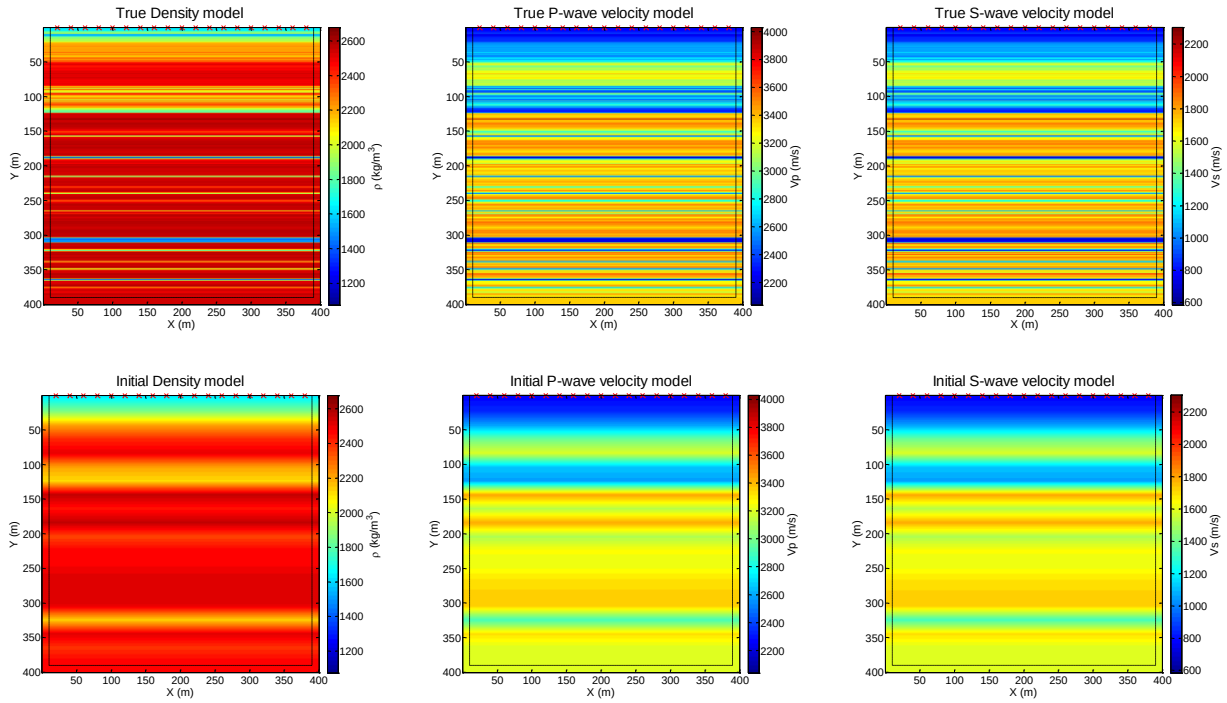

Figure 2: True models (top row) were used in generating shot records and initial models (bottom row) were used as starting point in the inversion. 19 seismic sources are positioned near the surface of the model at depth Y=5 m (red crosses) and from X= 20 m to X=380 m with 20 m spacing. Receivers were positioned at 1 m depth and extend from X=20 m to X=380 m at 1 m spacing.

PRODUCTION OF SYNTHETIC SHOT RECORDS

We used high resolution velocity and density models (Figure 2, top) to produce 19 synthetic shot records (no absorption) that will be treated as our field measurements $\mathbf{u}^{\mathbf{obs}}$ in the inversion. We positioned sources and receivers near the surface of the model from X=20 m to X=380 m buried at 5 m and 1 m depths, respectively. Receivers are spaced at 1 m and sources at 20 m intervals. Positions of seismic energy sources are shown in Figure 2 (cross marks) on the surface of the models. For this experiment, we selected explosive point sources as our seismic energy type and Ricker wavelet with central frequency $f_c = 80$ Hz to represent source function. We applied free surface conditions to the surface of the models and perfectly matched layers (PMLs) absorbing boundary conditions (Komatitsch and Martin, 2007) to the bottom and two side of the models demonstrated by dashed lines in Figure 2. We allocated 25 grid cells for PML zone to fully absorb a propagating wave with dominant frequency of 80 Hz and propagation velocity of 3000 m/s near the boundaries of the model. To simulate shot records, we selected FD order $n = 4$, a time stepping of $dT = 0.05$ ms and total recording time $T = 0.5$ s. We recorded both the vertical and horizontal components of the particle velocity field at each geophone location. Figure 3 shows an example of vertical and horizontal components of receiver recordings in the forward modelling part of this analysis (shot #10).

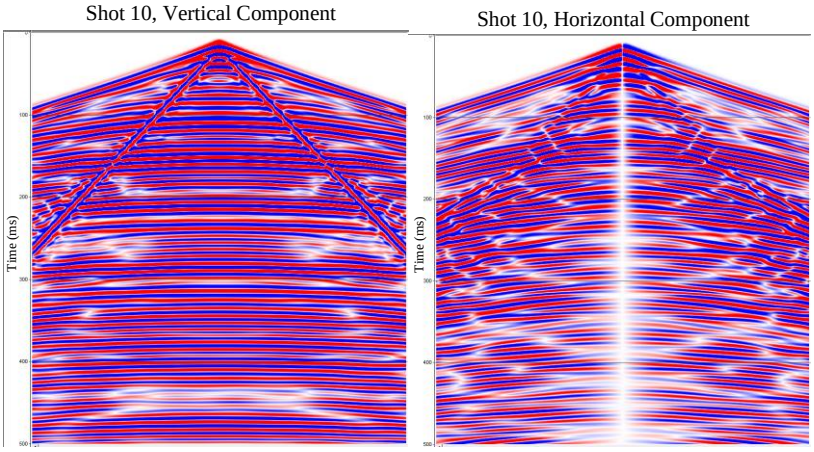

Figure 3: Vertical component (left) and horizontal component (right) of the receiver recordings ($\mathbf{u}^{\mathbf{obs}}$) at source location X=200 m (shot number 10). Receivers are positioned at 1 m intervals near the surface of the model (depth=1 m) from X=20 m to X=380 m.

FULL WAVEFORM INVERSION

Starting with initial models displayed in Figure 2 (bottom), we inverted synthetic shot records for elastic parameters V_P ,V_S and ρ using FWI open source program IFOS2D (Köhn, 2011) developed by Geophysical Institute (GPI) at Karlsruhe Institute of Technology (KIT). We used similar source-receiver configuration and wavelet characteristics (explosive point source with Ricker shape) as with the synthetic shot production stage. We allowed the algorithm to update each model from iteration one. The Hessian matrix for each shot was approximated by the algorithm following the approach described by Shin et al. (2001). To compute gradients we set the program to use preconditioned conjugate gradient (PCG) algorithm. The algorithm uses a parabolic line search method (Sourbier et al., 2009a,b, Brossier, 2009 and Nocedal and Wrigth,1999) to compute the step lengths. We also set up the program to use frequency filtering in the inversion. We started the inversion with a low pass frequency filter (10 Hz) applied to measured and simulated data and incremented it by 10 Hz up to an end frequency of 80 Hz at final inversion iteration.

Figure 4 shows the final results of the inversion (iteration 131) for elastic parameters ρ ,V_P and V_S . Comparing the inversion results with the starting models (Figure 2, bottom), it is evident that we have improved the initial model values by applying the inversion program. Another comparison can be made between inverted and true models demonstrated in Figures 4 and 2 (top). This comparison shows that we have been able to reconstruct many of the contrasting layer boundaries within the available seismic bandwidth.

A better comparison between inverted and true elastic parameters can be made by extracting a 1D log curve from inverted models and superimposing it on true and initial log displays. Figure 5 represents true, initial and inverted log curves for V_P ,V_S and ρ at the location of shot number 10 (X= 200 m) at the centre of the model. Main coal seam layers can be identified on true density log (black) curve as intervals with exceptionally lower density values. In spite of underestimating the true parameters at coal seam intervals, inverted velocity and density values have captured the main character (parameter fluctuations) of the true logs as demonstrated in Figure 5.

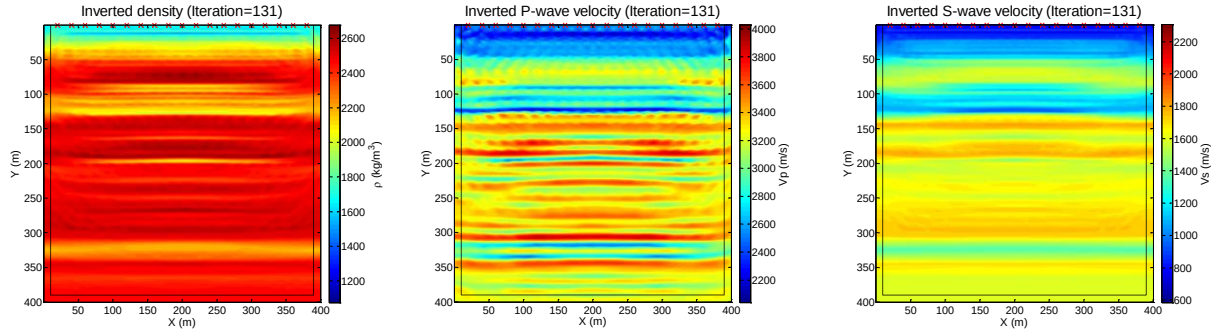

Figure 4: Final full waveform inversion results for elastic parameters ρ ,V_P and V_S .

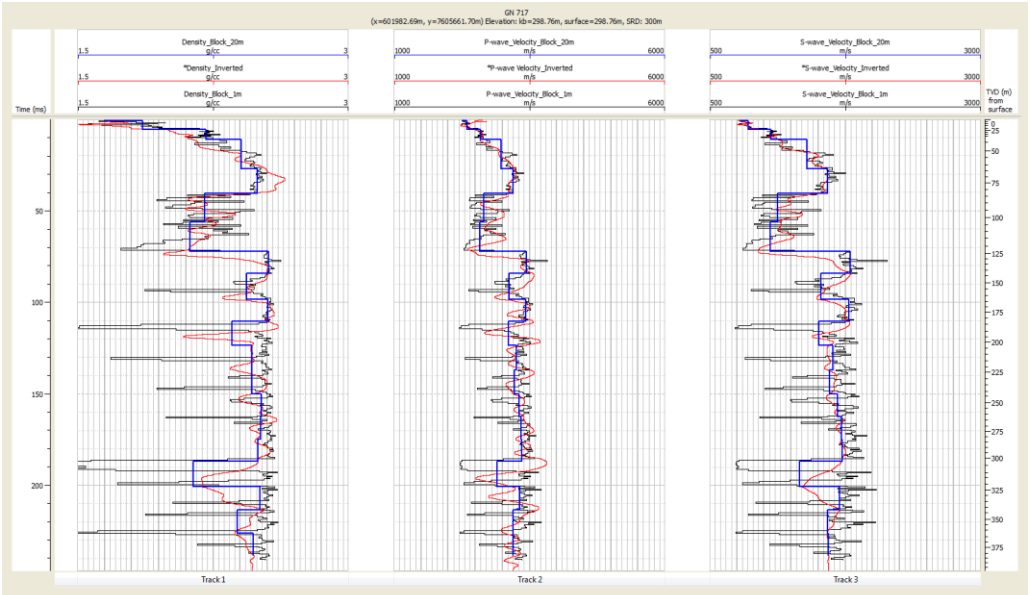

Figure 5: Final inversion results for V_P ,V_S and ρ at the centre of the model (X=200 m). Although underestimated at coal seam intervals, inverted parameters appear to capture the fluctuations in true logs.

Figure 6 demonstrates simulated seismograms (vertical and horizontal components) for shot number 10 (X=200 m) at the final iteration 131. A comparison between simulated seismograms in Figure 6 and observed data ($\mathbf{u}^{\mathbf{obs}}_{X=200}$) displayed in Figure 3 shows that the elastic contrast at the interfaces has been captured for the majority of layer boundaries on the vertical component. However, there is a mismatch between the horizontal components for recorded times below T=300 ms.

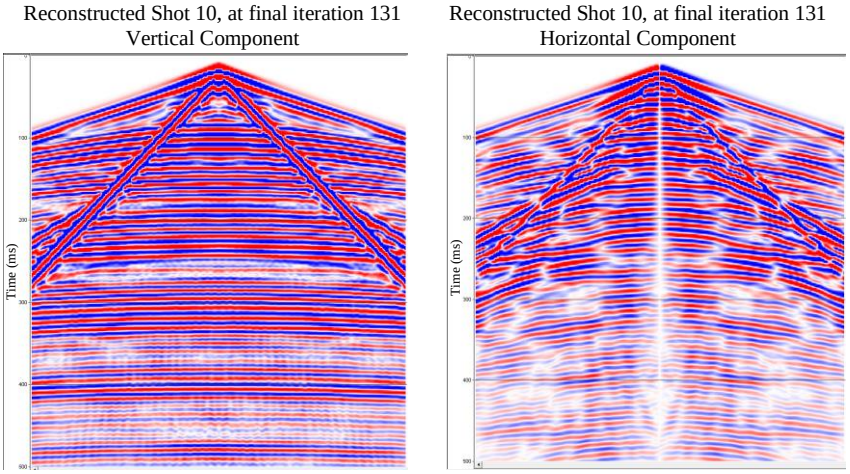

Figure 6: Vertical (left) and horizontal (right) components of the simulated seismograms at source location X=200 m (shot number 10) at iteration 131.

CONCLUSIONS

We examined the application of full (elastic) waveform inversion method on a synthetic dataset generated over the surface of a 2D earth model that was built using borehole log measurements in a coal bearing strata in Goonyella mines in Queensland. Our main objective was to evaluate the potential enhancement of estimated V_P , V_S and ρ parameters (with respect to initial values) through the application of FWI method to a dataset recorded over a short spread (360 m) of surface receivers. Despite using a short receiver array (array length ≈ maximum depth), we were able to improve the initial models and reconstruct a reasonable number of layer boundaries and parameter fluctuations for both the velocities and the density. However, we were unable to capture full details of elastic parameter variation in coal layers at mainly deeper intervals. This can be related to the absence of long offset data in our survey that can be used to retrieve the large and intermediate wavelengths of the 2D structure in our experiment (Mora, 1987 and 1988, Pratt and Worthington, 1990, Pratt et al., 1996). Increasing the source receiver offset in a field experiment will improve the estimated parameters, however, it may also raise a number of challenges such as the acquisition costs (source power, array length and number of channels), access related issues and computing power required for the inversion. The application of FWI for coal characterisation and for resolving mining hazards ahead of the long wall face is still in early experimental stage. However constant improvements in computing hardware and inversion software will enable full implementation of FWI for coal exploration in the near future.

REFERENCES

Akcelik, V., 2002, Multiscale Newton-Krylov methods for inverse acoustic wave propagation: Ph.D. thesis, Carnegie Mellon University.

Askan, A., Akcelik, V., Bielak, J., and Ghattas, O., 2007, Full waveform inversion for seismic velocity and anelastic losses in heterogeneous structures: Bulletin of the Seismological Society of America, 97, 1990–2008.

Askan, A., and Bielak, J., 2008, Full anelastic waveform tomography including model uncertainty: Bulletin of the Seismological Society of America, 98, 2975–2989.

Brossier, R., 2009, Imagerie sismique á deux dimensions des milieux visco-élastiques par inversion des formes d'ondes: développements méthodologiques et applications: PhD thesis, Universite de Nice - Sophia Antipolis.

Castagna, J. P., Batzle, M. L., Eastwood, R. L., 1985, Relationships between compressional-wave and shear-wave velocities in clastic silicate rocks: Geophysics, 50, 571–581.

Crase, E., Pica, A., Noble, M., McDonald, J., and Tarantola, A., 1990, Robust elastic non-linear waveform inversion: Application to real data: Geophysics, 55, 527–538.

Epanomeritakis, I., Akçelik, V., Ghattas, O., and Bielak, J., 2008, A Newton- CG method for large-scale three-dimensional elastic full waveform seismic inversion: Inverse Problems, 24, 1–26.

Hatherly, P.J., Urosevic, M., and Zhou, B., 2008, Seismic Inversion for Geotechnical Properties Relevant to Coal Mining: Proceedings of the symposium on the Application of Geophysics to Engineering and Environmental Problems, 21 , no. 1, 577-584.

Köhn, D., 2011, Time domain 2D elastic full waveform tomography: Ph.D. thesis, Kiel University.

Komatitsch, D., and Martin, R., 2007, An unsplit convolutional perfectly matched layer improved at grazing incidence for the

seismic wave equation: Geophysics, 72(5),155 – 167.
Marfurt, K., 1984, Accuracy of finite-difference and finite-elements modelling of the scalar and elastic wave equation: Geophysics, 49, 533–549.
Menke, W., 1984, Geophysical data analysis: Discrete inverse theory: Academic Press, Inc.
Min, D. J., Shin, C., Pratt, R. G., and Yoo, H. S., 2003, Weighted-averaging finite- element method for 2D elastic wave equations in the frequency domain: Bulletin of the Seismological Society of America, 93, 904–921.
Mora, P. R., 1987, Nonlinear two-dimensional elastic inversion of multi-offset seismic data: Geophysics, 52, 1211–1228.
Mora, P. R., 1988, Elastic wavefield inversion of reflection and transmission data: Geophysics, 53, 750–759.
Nocedal, J., and Wright, S. J., 1999, Numerical optimization: Springer.
Pratt, R. G., and Worthington, M. H., 1990, Inverse theory applied to multisource cross-hole tomography, Part 1: Acoustic wave-equation method: Geophysical Prospecting, 38, 287–310.
Pratt, R. G., Song, Z. M., Williamson, P. R., and Warner, M., 1996, Two-dimensional velocity model from wide-angle seismic data by wavefield inversion: Geophysical Journal International, 124, 323–340.
Pratt, R., Gao, F., Zelt, C., and Levander, A., 2002, The limits and complementary nature of traveltime and waveform tomography: International Conference of Sub-basalt imaging, Expanded Abstracts, 181–182.
Shin, C., Jang, S., and Min, D. J., 2001, Improved amplitude preservation for prestack depth migration by inverse scattering theory: Geophysical Prospecting, 49, 592–606.
Sourbier, F., Operto, S., Virieux, J., Amestoy, P., and L'Excellent, J. Y., 2009a, FWT2D: A massively parallel program for frequency-domain full-waveform tomography of wide-aperture seismic data — Part 1: Algorithm: Computers and Geosciences, 35, 487–495.
Sourbier, F., Operto, S., Virieux, J., Amestoy, P., and L'Excellent, J. Y., 2009b, FWT2D: A massively parallel program for frequency-domain full-waveform tomography of wide-aperture seismic data — Part 2: Numerical examples and scalability analysis: Computers and Geosciences, 35, 496–514.
Tarantola, A., 1987, Inverse problem theory: Methods for data fitting and model parameter estimation: Elsevier Science Publ. Co., Inc.
Urosevic, M., Evans, B. J., and Hatherly, P. J., 1992, The improvement in seismic resolution by map and trace attribute analysis: Exploration Geophysics 23, 387-392.
Urosevic, M., Evans, B. J., and Walton, C., 2000, Imaging coal seam structure using 3-D seismic methods: Exploration Geophysics, 31 , no. 3, 509-514.
Urosevic, M., Hatherly, P. J., and Evans, B. J., 1992, The application of surface seismic to the detection of methane producing fractures in coal: Symposium on Coalbed Methane Research and Development in Australia, 2, 1-14.
Virieux, J., 1986, P-SV wave propagation in heterogeneous media, velocity stress finite difference method: Geophysics, 51, 889–901.